26 May 1995

ELSEVIER

Chemical Physics Letters 238 (1995) 65–70

CHEMICAL PHYSICS LETTERS

Ultrasensitive quadrature photopyroelectric quantum yield spectroscopy of $Ti^{3+}:Al_2O_3$. Evidence for domination of de-excitation mechanism by inter-configurational nonradiative transitions in an unthermalized manifold

Andreas Mandelis [a], Marek Grinberg [b]

[a] *Photothermal and Optoelectronic Diagnostics Laboratory, Department of Mechanical Engineering, University of Toronto, Toronto, Ontario, Canada M5S 1A4*

[b] *Institute of Physics, Nicolaus Copernicus University, 87-100 Torun, Poland*

Received 4 November 1994; in final form 13 February 1995

Abstract

The lock-in quadrature channel of photopyroelectric spectroscopy (PPES) was used in a novel ultrasensitive non-contact configuration to measure $Ti^{3+}:Al_2O_3$ crystal nonradiative quantum yield bulk spectra, $\eta_{NR}^{(b)}(\lambda)$, which were analyzed allowing for both inter- and intra-configurational decay pathways of the Ti^{3+} ion in a two-dimensional harmonic oscillator adiabatic model. They were found to be dominated by inter-configurational de-excitation of the highly vibronically excited Ti^{3+} ion above cross-over, in clear break with current theoretical practices in unthermalized systems.

The detailed understanding of the photo-excitation decay dynamics of opto-electronic solid state systems which exhibit strong electron–lattice coupling, such as the Ti^{3+} ion in sapphire [1], requires the dependable and accurate measurement of quantum yield spectra, $\eta_R(\lambda)$, throughout the electronically active region ($\lambda \lesssim 600$ nm for $Ti^{3+}:Al_2O_3$). Such measurements are usually difficult to perform quantitatively using optical detection means, as they require complicated and often inaccurate absolute detector calibration procedures such as the integrating sphere method, or knowledge of absolute ion concentrations [2]. In recent years, however, it has been well documented that photopyroelectric spectroscopy (PPES), a photothermal technique, can be readily used to measure absolute nonradiative quantum yield spectra [3], $\eta_{NR}(\lambda)$, which may be easily and conveniently transformed to quantitative absolute (radiative) quantum yields,

$$\eta_R(\lambda) = 1 - \eta_{NR}(\lambda). \quad (1)$$

Particularly in the case of $Ti^{3+}:Al_2O_3$, a tunable solid-state laser material, the measurement and interpretation of $\eta_{NR}(\lambda)$ is important in its own right, since it can be a unique tool for understanding the optical-to-thermal energy conversion pathways which ultimately limit laser performance. In this Letter, we describe a novel PPES experimental configuration with enhanced thermal-wave detection sensitivity over conventional photopyroelectric detection [4], which allows the measurement of $\eta_{NR}(\lambda)$ spectra on transparent, high-quality optical materials. Ti : sap-

SSDI 0009-2614(95)00373-8

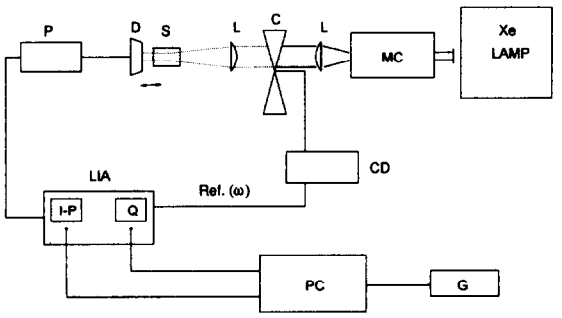

Fig. 1. Schematic of non-contact PPE spectrometer. MC: monochromator, L: lens, C: chopper, S: sample and (sample–detector distance) scanning stage, D: blackened PVDF detector, P: pre-amplifier with adjustable bandpass filters, LIA: lock-in amplifier (EG & G model 5210 in I-P and Q mode), CD: chopper driver, PC: computer for data acquisition, processing and theoretical analysis, G: graphics and plotter.

phire crystals occlude only minute quantities of thermally converted energy which cannot be detected reliably and quantitatively by conventional contacting PPES and other photothermal methods. The experimental $\eta_{NR}(\lambda)$ spectra were followed by a detailed analysis of the nonradiative dynamic processes occurring during the de-excitation of a two-level electronic system representing Ti^{3+} ions in Al_2O_3. A two-dimensional adiabatic configurational coordinate scheme was used where both intra- and inter-configurational relaxation processes were considered: the latter processes are neglected in conventional theories because the intra-configurational relaxation in unthermalized systems (i.e. higher-than-cross-over energies) is taken to be much more probable than nonradiative transitions which change the electronic state.

The experimental arrangement consisted of a simple Xe-lamp-based spectrometer described elsewhere [5] and is shown in Fig. 1. The PPES sensor element, made of polyvinylidene fluoride (PVDF), was decoupled from the flat polished surface of the $Ti^{3+}:Al_2O_3$ samples via micrometer stages, which allowed the air-gap distance between them to vary from ≈ 50 μm to 'infinity' (≈ 5 mm). The advantages of the non-contact geometry, Fig. 1, are (i) the absence of irreproducible thermal resistances (always present at the sample–PVDF interface in the contact mode); and (ii) the presence and the high degree of controllability of the airgap layer of variable thickness L. This allows for optimally efficient suppression of the direct optical heating mode of the sensor element itself (in-phase lock-in signal) and for easy, reproducible monitoring of the purely thermal-wave signal (lock-in quadrature) which is directly proportional to $\eta_{NR}(\lambda)$. It has been shown [5] that the total suppression of the much stronger in-phase signal (more than two orders of magnitude higher than the quadrature) allows the measurement of low optical-to-thermal energy conversion efficiencies η_{NR} in Ti:sapphire. To put the sensitivity of this new non-contact PPE spectrometer in perspective, Coufal measured phase shifts in the 0.1°–0.9° range with his fixed-thickness, contacting, thermal-wave 'phase shifter' with $\approx 0.1°$ phase resolution [4]. He was thus able to measure η_{NR} in the 0.55–0.9 range. By comparison, our method of quadrature detection using an absorption-free highly controllable variable-thickness thermal-wave phase shifter (i.e. the backing airgap layer) allowed the measurement of minute signals corresponding to phase shifts in the 0.02°–0.2° range with 0.015° phase resolution. Based on this order-of-magnitude improvement of quadrature PPES signals, in this work we labeled our novel PPE spectrometer 'ultrasensitive'. The foregoing phase resolution range is higher than the 0.5° photoacoustic (PA) phase resolution we have been able to achieve with the Ti:sapphire system. The PA phase is limited by microphonic (acoustic) noise, which is not present when the PVDF detector operates in the purely pyroelectric mode. The foregoing design amounts to an extension of the thermal-wave 'phase shifter' [4] to a thickness-adjustable, truly transparent phase shifter, also acting as pyroelectric dc drift compensator [6] and as thermal contact resistance eliminator [7]. Two pairs of different thicknesses and similar surface polishes of Ti:sapphire crystals were grown by the Czochralski pulling technique [5]. They had figures of merit (FOM) of 40 (unannealed) and 800 (annealed). FOM is defined as the optical absorption coefficient ratio at 490 and 820 nm. Optical absorption spectra, $\beta(\lambda)$, were obtained from the in-phase (IP)-PPE lock-in signal in the purely optical mode (PVDF detector at 'infinity') [5]. The non-contact sample–detector configuration yielded well-reproducible quadrature (Q)-PPE lock-in spectra in the purely thermal-wave mode (PVDF detector close to sample surface) [5], more than two orders of magni-

tude weaker than the IP signals. The low level of signal exhibited by the Q-PPE mode is characteristic of very weakly absorbing optical materials and was found to be equivalent to minimum phase shifts on the order of 0.02°. As a result of these ultra-small phase shifts detectable by the present non-contact spectrometer through the Q-channel, the contribution of the thermally very efficient surface absorptions closest to the detector element (due to the mechanical polishing process of laser-grade Ti:sapphire) proved to be dominant in certain spectral regions, especially below the electronic $^2T_{2g} \rightarrow {}^2E_g$ transition threshold. These surface absorptions were measured from each crystal pair to obtain a system of two spectra and two unknown parameters [8]: $\beta_b(\lambda)$, bulk optical absorption coefficient; and $A_s(\lambda)$, surface absorptance. Xe-lamp throughput-normalized transmission data from each crystal pair (thickness l_1, l_2) were used to obtain a system of two equations with two unknown parameters (β_b, A_s) of the form

$$\beta_b(\lambda) l_1 + 2A_s(\lambda) = S_1(\lambda), \tag{2a}$$

$$\beta_b(\lambda) l_2 + 2A_s(\lambda) = S_2(\lambda), \tag{2b}$$

where S_1 and S_2 are related to the normalized PPE spectroscopic signals, $V_\infty^{(j)}(\lambda)$, $j = 1, 2$. They can be written in terms of an analytical expression which also contains the (independently measured) optical reflectance spectrum [8],

$$\beta_b l_j + 2A_s = -\ln\left\{\frac{(1-R_s)^2}{2R_s^2 V_\infty^{(j)}} \times \left\{\left[1 + \left(\frac{2V_\infty^{(j)} R_s}{(1-R_s)^2}\right)^2\right]^{1/2} - 1\right\}\right\}, \tag{3a}$$

where

$$V_\infty^{(j)}(\lambda) = C_\infty^{(j)}(\omega; \lambda)/C_R(\omega; \lambda), \quad j = 1, 2, \tag{3b}$$

and $C_\infty^{(j)}$ (C_R) is the PPE transmission signal with (without) the sample of length l_j in place Upon solving the system for these parameters at each wavelength, the bulk absorption coefficient spectrum for each sample pair was obtained and is shown in

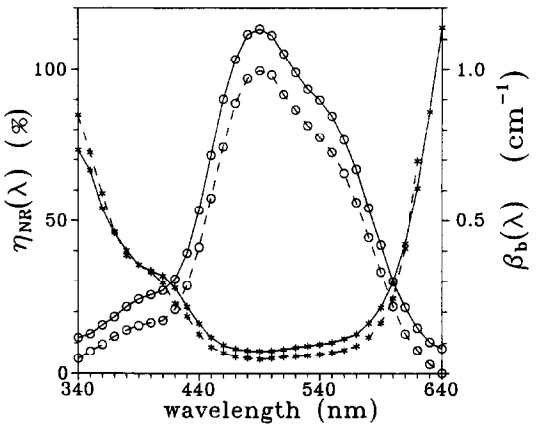

Fig. 2. Bulk optical absorption coefficient (circles) and nonradiative quantum yield (asterisks) spectra of two pairs of Ti:sapphire crystal rods from Union Carbide, Washougal, WA. Solid curves correspond to FOM = 40 (unannealed) samples; dashed curves correspond to FOM = 800 (annealed) samples. The experimental uncertainty in the $\eta_{NR}^{(b)}(\lambda)$ spectra was ±3%.

Fig. 2. The spectra are typical of the $Ti^{3+}:Al_2O_3$ system, consisting of a broad peak centered around 470 nm with a red-shifted shoulder. The peak is due to the $^2T_{2g} \rightarrow {}^2E_g$ transition broadened by phonons. The shoulder is the result of the Jahn–Teller splitting of the ^2E_g state [9]. For the FOM = 800 crystal pair, the bulk absorption becomes zero at ≈ 640 nm, in agreement with the minimum photon energy threshold required to induce an $^2T_{2g} \rightarrow {}^2E_g$ electron transition (≈ 6471 Å) [10]. The near-IR bulk absorption of the FOM = 40 crystals is intrinsic to as-grown Czochralski crystals and has been associated with Ti^{3+} ions in interstitial or defect sites close to native defects [11].

Thermal energy generation bulk $\eta_{NR}^{(b)}(\lambda)$ spectra were calculated from experimental Q-PPE lock-in spectra in the purely thermal-wave mode, using the imaginary part of the normalized equation for the PPE signal voltage [8],

$$V[\beta_b(\lambda), \eta_{NR}^{(b)}(\lambda)] = F_1[\beta_b(\lambda)] + \eta_{NR}^{(b)}(\lambda) F_2[\beta_b(\lambda)]. \tag{4}$$

F_1 and F_2 are complex functions of optical, thermal and geometric parameters of the system. The appropriate thermophysical values for the crystal, air, and pyroelectric detector were used [5]. Fig. 2 shows the

$\eta_{NR}^{(b)}(\lambda)$ spectra for the two pairs of crystals. The nonradiative quantum efficiencies of each pair of samples increase for $\lambda > 490$ nm. These have been attributed to residual additive absorptions due to the crystal surfaces with absorptance A_s and $\eta_{NR}^{(s)} = 1$, and to bulk, purely nonradiative defects [11], not related to the Ti^{3+} excited-state manifold. These effects have been discussed elsewhere [12]. The slightly higher $\eta_{NR}^{(b)}$ for the FOM = 40 crystal pair is also expected, since the higher density of bulk nonradiative defect centers in these crystals is capable of inducing enhancement of the nonradiative transition quantum yield, W_{NR}, from the metastable excited state ^2E. We have modelled the energetic structure of $Ti^{3+}:Al_2O_3$ taking into account a large Jahn–Teller $E \times \epsilon$ effect in the ^2E state and a small such effect in the ground $^2T_2$ state [1]. The significant nonlinear electron–lattice coupling found in the ^2E state [1] causes the double phonon structure of structure of the zero-phonon line in the absorption spectrum. The rate of phonon emission was calculated from the dynamics of the Ti : sapphire de-excitation [1], using, in addition, the probabilities for intra-configurational and inter-configurational nonradiative transitions P_{intra} and P_{inter}, respectively, inside the ground (g) and excited (e) manifolds, Fig. 3 (inset). The quantum yield of the system is obtained as follows [12]:

$$\eta_R[\hbar\Omega(\lambda), T] = \eta_R^n[\hbar\Omega(\lambda)]\eta_R^t(T), \tag{5}$$

where

$$\eta_R^t(T) \equiv \frac{P_{rad}^t}{P_{rad}^t + P_{nr}^t(T)} \tag{6}$$

is the quantum efficiency of the thermalized system, which generates the temperature dependence of η_R. P_{rad}^t and P_{nr}^t indicate the radiative and nonradiative probabilities responsible for system thermalization. Furthermore,

$$\eta_R^n \equiv \prod_{k=1}^{n(\hbar\Omega)} \frac{P(e)_{intra}^k}{P_{inter}^{kl} + P(e)_{intra}^k} \tag{7}$$

is the efficiency of the thermalization process which depends on the energy of the exciting photons.

Eq. (5) is of considerable significance. To appreciate its importance consider the relationship of the present model to what will be labelled 'the standard approach,' where the fast nonradiative internal conversion is not considered: Usually, it is assumed that the intra-configurational transitions are so fast that the depopulation of the highly excited vibronic states of the excited electronic manifold by inter-configurational relaxation to the ground state (internal conversion) is negligible [13]. It should be emphasized that there are no other electronic levels associated with the Ti^{3+} ion besides the ^2E-excited and $^2T_2$-ground electronic manifolds: The octahedrally coordinated Ti^{3+} ion contains only one electron in the d shell, which results in a very simple electronic structure of this system. On the other hand, other typical electronic manifolds such as the Fe^{2+} ion in porphyrin compounds with six electrons in the d shell, can undergo rapid intersystem crossing and quench the luminescence via their much more complex excited-state structures.

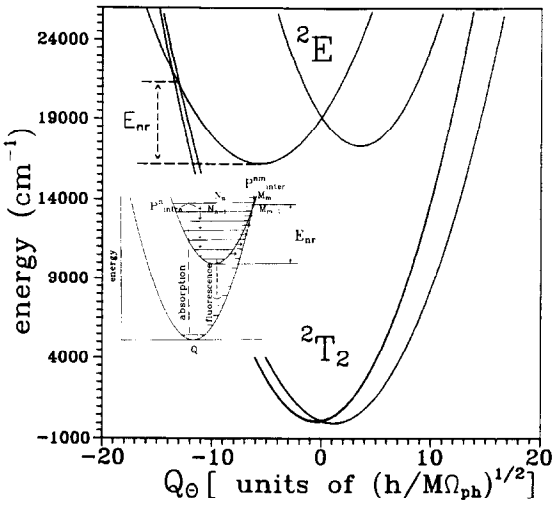

Fig. 3. Configurational coordinate diagram and vibronic structure of a two-electronic manifold system. Radiative transitions are indicated by dashed arrows; nonradiative processes are indicated by solid arrows. The classical barrier for nonradiative transitions, i.e. the cross-over energy, E_{nr}, is shown in the figure. The inset shows parameter definitions in Eqs. (5)–(8).

To obtain the quantum efficiency, $\eta_R^{Ti}(\lambda, T)$, of the Ti^{3+}, the nonradiative transition probability $P_{nr}^t(T)$ and the internal conversion probability $P(^2E \rightarrow {}^2T_2)_{inter}^{ij}$ were calculated according to Ref. [1], using a two-dimensional harmonic oscillator model

to describe the vibronic structure of the ground and excited electronic state manifolds. In the case of the Ti^{3+} ion, nonradiative transitions between the ^2E and $^2T_2$ electronic manifolds are allowed by the spin–orbit interaction [1] which mixes the electronic wavefunctions of the ^2E and $^2T_2$ states. Thus, the internal conversion time constant was determined from the calculated value of the spin–orbit matrix element: $\tau_{inter}^{-1} = 3 \times 10^{13}$ s^{-1} [1]. The probability of the radiative transition has been assumed to be equal to 0.26×10^6 s^{-1}, i.e. the inverse of the radiative decay time of Ti^{3+}:sapphire at zero temperature. $P(^2E)^n_{intra}$, the probability of intra-configurational nonradiative transition was assumed proportional to the vibronic quantum number of the initial vibronic state,

$$P(^2E)^n_{intra} = \tau_{intra}^{-1} n. \quad (8)$$

The value of τ_{intra} was treated as the only free parameter of the model. Simulations of the inter- and intra-configurational transition probabilities as functions of photon energy showed an increase in the probability of the internal conversion process with increasing energy, stronger than that predicted by a one-dimensional harmonic oscillator model because the significant nonlinear ^2E-state electron–lattice coupling causes the increase of vibronic wavefunction overlap integrals for energies of the initial state much smaller than those for linear coupling. The overall theoretical-computational result was that the radiative quantum yield starts to decrease for excitation wavelengths λ smaller than λ_{nr} ($= hc/E_{nr} = 480$ nm), with a slope which depends on the value of τ_{intra}.

To interpret the experimental PPES $\eta_{NR}^{(b)}(\lambda)$ spectra of $Ti^{3+}:Al_2O_3$, attention was focused in the spectral range 340 nm $< \lambda <$ 620 nm, where bulk absorption is dominant, Fig. 2. For $\lambda >$ 620 nm and $\lambda \lesssim$ 340 nm the measured η_{NR} is not related to the Ti^{3+} ions [12]. Fig. 4 shows that the experimental quantum yield derived from the PPE quadrature spectrum and Eq. (2) is almost constant and equal to 90% for 450 nm $< \lambda <$ 580 nm. The significant increase of $\eta_{NR}^{(b)}(\lambda)$ below 450 nm is related to the increased probability of the internal conversion process in the Ti^{3+} ion excited to high vibronic states of the ^2E electronic manifold. Since the parameters of

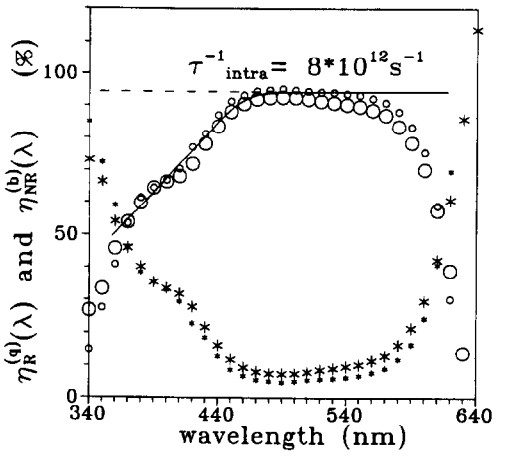

Fig. 4. Nonradiative and radiative transition efficiency spectra of FOM = 40 and 800 crystal pairs of $Ti^{3+}:Al_2O_3$. Quantum yields, $\eta_R(\lambda)$, are indicated by circles; nonradiative bulk quantum yields, $\eta_{NR}^{(b)}(\lambda)$, are indicated by asterisks. Small (large) size symbols represent the FOM = 800 (40) crystal pair. The experimental nonradiative quantum yields were obtained using PPE quadrature spectra in Fig. 2. Solid line: theoretical quantum yield calculated for $T = 300$ K. Jahn–Teller, phonon and E_{nr} energies, as well as nonlinearity coefficients for $^2T_2$ and ^2E electronic states were taken from Refs. [1,12]. The dashed line corresponds to the standard models [13] for which the internal conversion processes are negligible.

the configuration coordinate diagram, Fig. 3, and the phonon energies of the Ti^{3+} system were obtained self-consistently from the PPES optical mode (in-phase) data, Fig. 2 and Ref. [1], the best fits to both crystal pairs with FOM = 40 and 800 at $T = 300$ K gave $\tau_{intra} = 1.25 \times 10^{-13}$ s.

In conclusion, the complete theoretical and experimental spectral dependence of the bulk nonradiative quantum efficiency of the Ti^{3+} ion in sapphire was achieved as a result of our introduction of a novel, ultrasensitive non-contact PPE quadrature spectroscopy with superior phase resolution to other conventional photothermal techniques. A nonradiative de-excitation theory based on a two-dimensional configuration coordinate scheme was developed. The theory included the large Jahn–Teller $E \times \epsilon$ effect in the ^2E state and the strong nonlinear electron–lattice coupling found in the ^2E state. Both intra- and inter-configurational relaxation processes were considered. The experimental PPE $\eta_{NR}^{(b)}(\lambda)$ spectra were found to be dominated by interconfigurational de-ex-

citation of the highly vibronically excited Ti^{3+} ion above the cross-over energy E_{nr}, a clear departure from current theoretical practices regarding systems with simple electronic structures which cannot undergo rapid intersystem crossing to quench the luminescence. A one-parameter fit of the theoretical radiative quantum yield to the complement of the PPE $\eta_{NR}(\lambda)$ spectrum gave the intra-configurational relaxation time constant $\tau_{intra} = 1.25 \times 10^{-13}$ s for the $Ti^{3+}:Al_2O_3$ system, an otherwise not easily accessible parameter. The present combined PPE experimental/theoretical approach strongly suggests the need for re-examination of the conventional dynamical nonradiative de-excitation models, with respect to the importance of the interconfigurational internal conversion processes for all systems strongly coupled to the lattice.

This work was financially supported by the Natural Sciences and Engineering Research Council of Canada through a Strategic Grant.

References

[1] M. Grinberg, A. Mandelis, K. Fjeldsted and A. Othonos, Phys. Rev. B 48 (1993-I) 5922, 5935.
[2] R.S. Quimby and W.M. Yen, Opt. Letters 3 (1978) 181.
[3] H. Coufal and A. Mandelis, Ferroelectrics 118 (1991) 379, and references therein.
[4] H. Coufal, Appl. Phys. Letters 45 (1984) 516.
[5] A. Mandelis, J. Vanniasinkam, S. Buddhudu, A. Othonos and M. Kokta, Phys. Rev. B1 48 (1993-II) 6808.
[6] S. Buddhudu, A. Mandelis, B. Joseph and K. Fjeldsted, Opt. Mater. 3 (1994) 115.
[7] A. Mandelis and A. da Silva, Ferroelectrics, in press.
[8] J. Vanniasinkam, A. Mandelis, S. Buddhudu and M. Kokta, J. Appl. Phys. 75 (1994) 8090.
[9] P.F. Moulton, J. Opt. Soc. Am. B 3 (1986) 125.
[10] B.F. Gachter and J.A. Koningstein, J. Chem. Phys. 60 (1974) 2003.
[11] P. Lacovara, L. Esterowitz and M. Kokta, IEEE J. Quantum Electron. QE-21 (1985) 1614.
[12] M. Grinberg and A. Mandelis, Phys. Rev. B1 49 (1994) 12496.
[13] F.K. Fong, ed., Topics in applied physics, Vol. 15. Radiationless processes in molecules and condensed phases (Springer, Berlin, 1976).